2021 43rd Annual International Conference of the
IEEE Engineering in Medicine & Biology Society (EMBC)
Oct 31 - Nov 4, 2021. Virtual Conference

Noninvasive Cardiac Transmembrane Potential Imaging via Global Features Based FISTA Network

Linsheng Cheng and Huafeng Liu*

***Abstract*— Noninvasive electrophysiological imaging plays an important role in the clinical diagnosis and treatment of heart diseases over recent years. Transmembrane potential (TMP) is one of the most important cardiac physiological signals, which can be used to diagnose heart disease such as premature beat and myocardial infarction. Considering the nonlocal self-similarity of TMP distribution and integrating traditional optimization strategy into deep learning, we proposed a novel global features based Fast Iterative Shrinkage/Thresholding network, named as GFISTA-Net. The proposed method has two main advantages over traditional methods, namely, the l1-norm regularization helps to avoid overfitting the model on high-dimensional but small-training data, and facilitates embedded the spatio-temporal correlation of TMP. Experiments demonstrate the power of our method.**

I. INTRODUCTION

While the body surface potential (BSP) recordings have been able to provide noninvasive observations of electrical activity of the heart, interpreting BSP data is difficult due to its poor ability to pinpoint the electrical functioning inside the muscular tissue of the heart, and the fact that transmiting through the torso blurs the signals. Cardiac transmembrane potential (TMP) describes the state of excitation and cardiac action directly, which is a tight coulping of electrical and mechanical functions in the heart, thus is of great clinical interest, i.e. it can be used to diagnose the myocardial ischemia and infarction clinically.

In this paper, we address a problem of reconstructing the detailed images of spatiotemporally TMP distribution of the heart from BSP recordings, which provide a safer manner. Generally speaking, these non-invasive reconstruction methods can be divided into two main groups: 1) model-based methods, 2) deep learning/machine learning (DL/ML) based methods.

The difficulty facing here is that the number of unobserved variables greatly exceeds the number of measurements. Therefore, additional regularization constraints, reflecting specific domain properties or assumptions, must be introduced to overcome the ill-posedness of the BSP inverse problems.In [1], a model-based state space framework was proposed to reconstruct volumetric TMP dynamics inside the myocardium from noninvasive BSP recordings. Another approaches which imposed a sparse-based constraint with l1-norm have been proposed such as total variation (TV) regularization [2]. And in order to take into account the spatial and temporal correlation of TMP, graph-based TV was proposed to improve the accuracy of reconstruction [3].

Linsheng Cheng and Huafeng Liu are with State Key Laboratory of Modern Optical Instrumentation, Zhejiang University, Hangzhou 310027, China

*Corresponding author (Email: liuhf@zju.edu.cn)

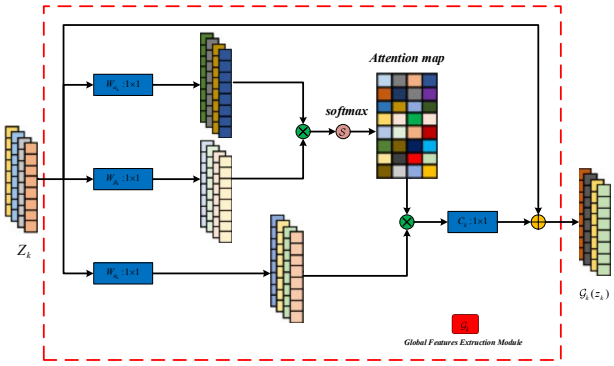

Fig. 1. Detailed illustration of global features extraction module.

However, these approaches rely on the hand-craft regularization and the iterations are time-consuming. Alternatively, deep learning has been applied to solve BSP inverse problems in recent years.

Dhamala J et al used a generative variational auto-encoder (VAE) for the reconstruction of TMP [4] and later the method based on graph convolutional neural network was proposed to process the non-Euclidean space data of TMP [5].

This paper proposes a model-based deep learning technique to solve the inverse problems in order to combine the physical interpretation and convergence theory of traditional fast iterative threshold shrinkage algorithm with the powerful expression ability of deep learning. By unfolding the iterative steps into repetitive blocks, replacing the soft-thresholding steps with convolution neural networks (CNN) and using global feature extraction module to extract nonlocal information, we introduce a novel global features based Fast Iterative Shrinkage/Thresholding network, referred to as GFISTA-Net. Main contributions of this paper include:

- We build a CNN to solve the proximal mapping with sparse constraint regularization. One GFISTA block corresponds to one iteration of the constraint-based method.
- Add a global feature extraction module into GFISTA block to make better use of the spatio-temporal correlation of TMP.
- GFISTA-Net obtains state-of-the-art results compared with other algorithms by adding a series of improvements according to the characteristics of TMP sequences.

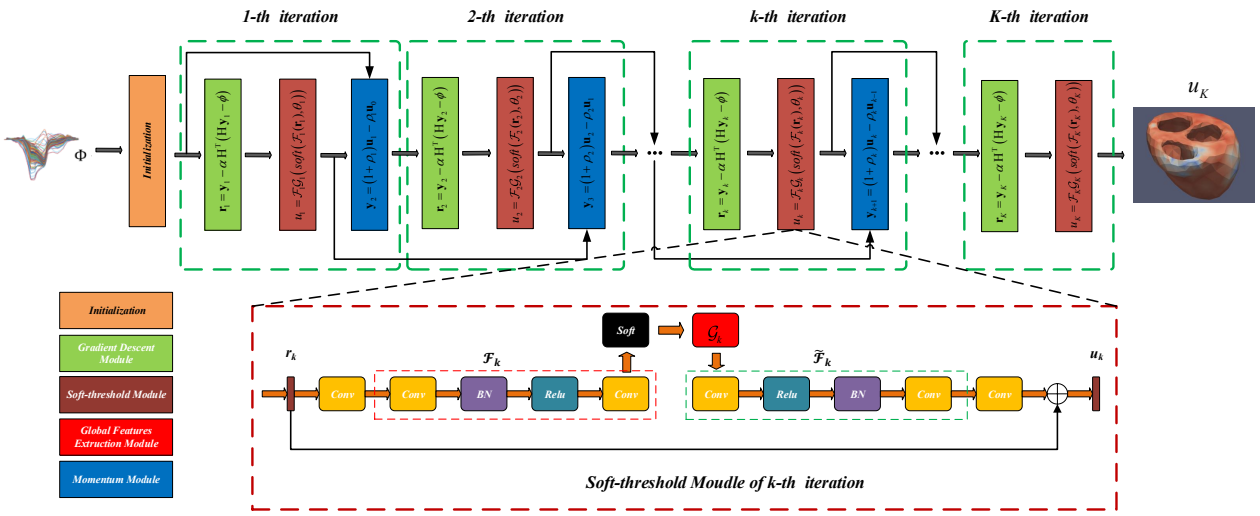

Fig. 2. Schematic diagram of GFISTA-NET network structure.

II. METHOD

A. BSP-TMP Relationship

Forward model: Following the work in [6], forward model from BSP to TMP can be expressed as a linear fomulation:

$$\phi = \mathrm{H}\boldsymbol{u} \tag{1}$$

where ϕ denotes measurements of BSP record with lead m. $\boldsymbol{u}$ is the distribution of TMP to be reconstructed and the number of nodes on heart is n. H is the transfer matrix which contains the relationship in heart-torso geometric model.

Inverse problem: Because the number of leads measured on body surface is far less than the nodes on the heart, the ECG inverse problem that reconstruct TMP from BSP is rank deficiency and ill-posed. Based on the prior knowledge of TMP, it is useful that adding sparse constraints to overcome the ill-poseness:

$$\min_{u} \frac{1}{2}\|\mathrm{H}\boldsymbol{u} - \boldsymbol{\phi}\|_2^2 + \lambda\|\Psi\boldsymbol{u}\|_1 \tag{2}$$

The l_1 norm guarantees sparseness. Ψ is one of transform operators, such as total variance or wavelet operator based on different data information, and λ is the regularization coefficient.

B. Based Method

FISTA: Frequently, Equation 2 cannot be solved straightforward. ISTA is a classic method to solve this problem above. And fast Iterative Shrinkage-Thresholding Algorithm (FISTA) [7] is a faster version of ISTA. FISTA uses the following iterative steps:

$$\boldsymbol{u}_k = \mathcal{T}_\theta\left(\boldsymbol{y}_k - \alpha\mathrm{H}^{\mathrm{T}}\left(\mathrm{H}\boldsymbol{y}_k - \boldsymbol{\phi}\right)\right) \tag{3}$$

$$t_{k+1} = \frac{1+\sqrt{1+4\left(t_k\right)^2}}{2} \tag{4}$$

$$\boldsymbol{y}_{k+1} = \boldsymbol{u}_k + \left(\frac{t_k - 1}{t_{k+1}}\right)\left(\boldsymbol{u}_k - \boldsymbol{u}_{k-1}\right) \tag{5}$$

where $\mathcal{T}_\theta$ is the soft threshold operator. $\boldsymbol{k}$ is the current number of iterations. α is the step length of gradient descent. $\boldsymbol{y}_k$ is an auxiliary variable, which is a linear conbination of the previous two estimates $\boldsymbol{u}_{k-1}$, $\boldsymbol{u}_{k-2}$ and is a new starting point for next iteration.

C. GFISTA-Net

In order to integrate the advantages of FISTA and deep learning, we proposed a novel network named as GFISTA-Net. Next, we elaborate the structure of GFISTA-Net.

Gradient Descent Module $\boldsymbol{r}_k$: This module updates the reconstructed TMP acording to Equation 6. The $\boldsymbol{y}_k$ is the output of the last block.

$$\boldsymbol{r}_k = \boldsymbol{y}_k - \alpha\mathrm{H}^{\mathrm{T}}\left(\mathrm{H}\boldsymbol{y}_k - \boldsymbol{\phi}\right) \tag{6}$$

Soft-threshold Module $\boldsymbol{u}_k$: Based on Equation 7, noise and artifacts of the results $\boldsymbol{r}_k$ can be greatly improved. The step from $\boldsymbol{r}_k$ to $\boldsymbol{u}_k$ is designed as a convolution neural networks and the form of the proximal mapping operator is preserved. The transform operator $\boldsymbol{\Psi}$ in Equation 2 is generally a fixed constraint form, but $\boldsymbol{\Psi}$ and $\boldsymbol{\Psi}^T$ are regarded as the learnable nonlinear operators $\mathcal{F}$ and $\widetilde{\mathcal{F}}$.

$$\begin{aligned} &\boldsymbol{u}_k = prox_{\theta_k}(\boldsymbol{r}_k) = \widetilde{\mathcal{F}}_k\left(soft\left(\mathcal{F}_k(\boldsymbol{r}_k), \theta_k\right)\right) \\ &\widetilde{\mathcal{F}} \circ \mathcal{F} = \mathcal{I} \end{aligned} \tag{7}$$

where $soft\left(.\right)$ is the soft-threshold function. The $\mathcal{F}$ operator is replaced with structure of Conv-ReLU-Conv and the $\widetilde{\mathcal{F}}$ is the orthogonal symmetric form of $\mathcal{F}$. $\mathcal{I}$ is the unit matrix to guarantee the orthogonality.

Based on the ResNet [8], Equation 7 is modified to the form of residual.

$$\begin{aligned} &Res_k = \widetilde{\mathcal{F}}_k\left(soft\left(\mathcal{F}_k(\boldsymbol{r}_k), \theta_k\right)\right) \\ &\boldsymbol{u}_k = \boldsymbol{r}_k + Res_k \end{aligned} \tag{8}$$

Global Features Extraction Module $\mathcal{G}_k$: Convolution only pays attention to the area of the neighboring kernel

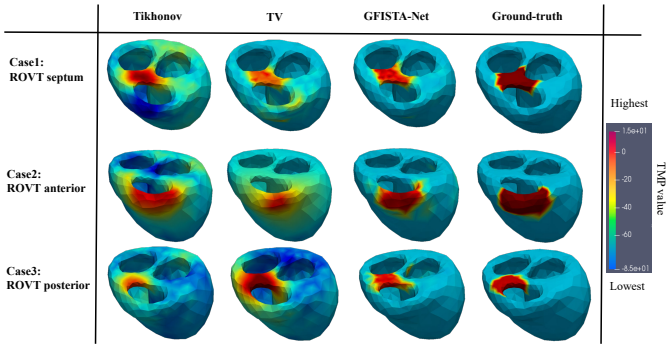

Fig. 3. Three-dimensional TMP maps reconstructed by three different methods when the heart initiates ectopic pacing in different locations, where the color red indicates the earliest activation and the blue indicates the latest activation.

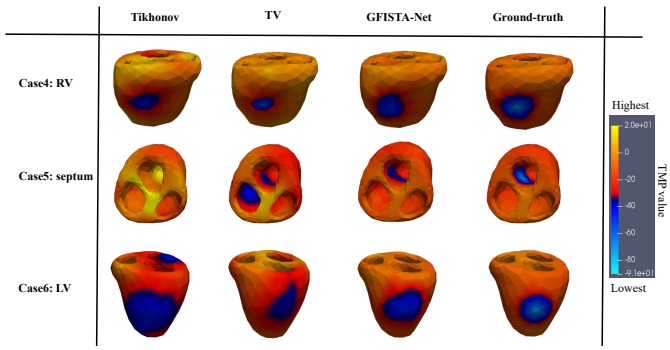

Fig. 4. Three-dimensional TMP maps reconstructed by three different methods of infarcts in different locations. Blue parts indicate infarction, black parts represent ischemia, and yellow parts are normal cells.

size, thus it ignores the contribution of other global areas to the current area. Therefore, The attention mechanism is adopted to extruct global features. On the strength of [9], the caculation process can be showm as:

$$\mathcal{G}_k = \mathcal{S}\left(\left(W_{\alpha_k}\left(z_k\right)\right)^T W_{\beta_k}\left(z_k\right)\right) W_{\theta_k}\left(z_k\right) + \boldsymbol{z}_k \tag{9}$$

where $\mathcal{G}_k$ means the attention block. $\mathcal{S}$ is softmax function. $\boldsymbol{z}_k$ are feature maps after the process of $soft\left(\mathcal{F}_k(\boldsymbol{r}_k), \theta_k\right)$. W_* are the weight matrixs which are learnable parameters in each block. The whole process is shown in Fig 1.

The attention block $\mathcal{G}_k$ is applied to the feature maps $\boldsymbol{z}_k$. The process in Equation 8 can be modified to Equation 10.

$$Res_k = \widetilde{\mathcal{F}}_k \mathcal{G}_k\left(soft\left(\mathcal{F}_k(\boldsymbol{r}_k), \theta_k\right)\right) \tag{10}$$

Momentum Module $\boldsymbol{y}_k$: FISTA converges faster than ISTA because of adopting the update weights of two last reconstructed results as in Equation 4 and 5. In FISTA-Net, we simplify this step by replacing $\frac{t_k - 1}{t_{k+1}}$ with a learnable parameter ρ_k and use the updated ρ_k to calculate $\boldsymbol{y}_k$. The step is as follows:

$$\begin{aligned} \boldsymbol{y}_1 &= \boldsymbol{u}_0 \\ \boldsymbol{y}_{k+1} &= \boldsymbol{u}_k + \rho_k\left(\boldsymbol{u}_k - \boldsymbol{u}_{k-1}\right) \end{aligned} \tag{11}$$

Network Structure: Integrating four parts of gradient descent module, soft-threshold moudle, global features extruction moudle and momentum moudle, the final network structure of GFISTA-Net is shown in Fig 2. Each phase corresponds to one iteration of FISTA.

Three requirements should be taken account into the loss function of GFISTA-Net. $\mathcal{L}_{\text{mse}}$ is the MSE loss of the reconstructed result of the final phase relative to the ground truth. $\mathcal{L}_{\text{sym}}$ is a symmetry loss and designed for the necessariness of $\widetilde{\mathcal{F}} \circ \mathcal{F} = \mathcal{I}$ in each phase. $\mathcal{L}_{\text{spa}}$ is a sparse constraint. Finally, the total loss function $\mathcal{L}_{\text{total}}$ is a weighted superposition of these three different losses.

$$\begin{aligned} \mathcal{L}_{\text{total}} &= \beta_1 \mathcal{L}_{\text{mse}} + \beta_2 \mathcal{L}_{\text{sym}} + \beta_3 \mathcal{L}_{\text{spa}} \\ \mathcal{L}_{\text{mse}} &= \left\|\boldsymbol{u}_k - \boldsymbol{u}\right\|_2^2 \\ \mathcal{L}_{\text{sym}} &= \frac{1}{K}\sum_{k=1}^{K}\left\|\widetilde{\mathcal{F}}_k\left(\mathcal{F}_k\left(\boldsymbol{r}_k\right)\right) - \boldsymbol{r}_k\right\|_2^2 \\ \mathcal{L}_{\text{spa}} &= \frac{1}{K}\sum_{k=1}^{K}\left\|\mathcal{F}_k\left(\boldsymbol{r}_k\right)\right\|_1 \end{aligned} \tag{12}$$

where K is the phase number of GFISTA-Net. β_* are fixed hyperparameters. we set $\beta_1 = 1$, $\beta_2 = 0.01$ and $\beta_3 = 0.001$ in this paper.

III. EXPERIMENTS AND RESULTS

A. Dataset and Implementation Details

In this section, we evaluate the accuracy of the proposed algorithm for reconstructing TMP. Based on the MRI, we can get the personalized heart-torso model. H is obtained by the boundary finite element method based on the bidomain model. The total 400 groups of TMP-BSP data pairs with different pacing site and different infarct sites and size are used in this paper. The size of one group of TMP is $697*500$ and it is $64*500$ for BSP, where 697 is the number of nodes on the heart ($n = 697$) and 64 is the number of leads on the body surface ($m = 64$).

We divided the training set, test set, and validation set according to the principle of 8: 1: 1. The final amount of data is 160,000 for the training set and 20,000 for the test and validation sets. The network is based on the Tensorflow platform, the operating environment is python 3.6, and the GPU model is a single TITAN RTX GPU (24GB). The optimization algorithm is Adam algorithm. The batch size is 128, the learning rate is 0.001, the number of trainings N = 500, and the total number of iterations in a single training K = 11. GFISTA-Net and ISTA-Net [10] do the same settings.

B. Experiments on Ventricular Ectopic Pacemaker

This part of the experiment was designed to verify the reconstruction performance of our method when the heart appears ectopic pacing. Considering that common ectopic

ventricular pacing occurs in the right ventricular outflow tract (ROVT), qualitative analysis results of these cases are shown in the Fig 3 particularly. Different ventricular ectopic pacemakers were set at septum, anterior and posterior of RVOT in this part. The red part is the first activated part, which can be seen as the ectopic pacemaker, and the blue or cyan part is not activated yet. The Tikhonov method cannot clearly indicate the propagation wavefronts of the pacing site in the initial stage when pacing occurs. Although the TV method performs better, the wavefront shapes aren't close enough to ground truth. The results of GFISTA-Net accurately reveal the location of the pacemakers and show the closest propagation wavefront shapes.

C. Experiments on Infarct Scar Reconstruction

In the TMP sequence, the spatial distribution of the potential of a certain frame can clearly indicate the low voltage area caused by the infarction. Fig 4 shows the reconstruction of the TMP in three different infarct locations. The time node shown is about 200ms after the pacing, that is, the time when the ventricular depolarization is completed and the ECG is in the ST segment. Tikhonov and TV methods have problems with over-smoothing of TMP spatial distribution due to the usage of priori operators that does not completely conform to TMP spatial-temporal distribution. Particularly, there is not a clear infarcted area in case 5 or multiple infarcted centers in case 6 according to the reconstruction results using Tikhonov method. Although the results of TV method is better than Tikhonov, it is still not good enough. The TV method tends to reduce the range of lesions in case4, have an incorrect infarct location in case 5 and increase the range in case 6. Meanwhile, the proposed GFISTA-Net has good adaptability to the noise and the learned physiological priori is suitable for TMP. GFISTA-Net clearly indicate the location of the infarcted nucleus and ischemic zone because of our global features extraction module to reduce the sensitivity to noise.

D. Comparison Experiments

We perform comparison experiments on our dataset to evaluate models on TMP reconstruction. TABLE I is a quantitative comparison of the four methods. The indicators are relative error (RE) and structural similarity (SSIM). The results shown are the statistical results of 20,000 data in the test set, including the mean and standard deviation. It can be seen that GFISTA-Net has improved significantly compared to traditional methods and the original ISTA-Net.

TABLE I

RESULTS OF GFISTA-NET COMPARED WITH TRADITIONAL REGULARIZATION-BASED TIKHONOV AND TV METHODS AND THE ORIGINAL ISTA-NET. RE AND SSIM ARE ADOPTED.

Method	RE	SIMM
Tikhonov	0.2125 ± 0.0203	0.5027 ± 0.0521
TV	0.1726 ± 0.0165	0.5371 ± 0.0470
ISTA-Net	0.0755 ± 0.0194	0.6151 ± 0.0886
GFISTA-Net	$\mathbf{0.0613 \pm 0.0185}$	$\mathbf{0.7013 \pm 0.0752}$

IV. CONCLUSIONS

Based on the body surface potential maps, we proposed a GFISTA-Net to reconstruct the distribution of TMP noninvasively. The method adopts attention mechanism to extract global features considering the nonlocal similarity of TMP. GFISTA-Net incorporates a momentum module so as to have better reconstruction accuracy and converge faster than ISTA-Net. Due to the fusion of FISTA and neural networks, Our algorithm not only has reliable physical interpretation and convergence theory but also has good flexibility and generalization performance. All the improvements in the network make GFISTA-Net outperform the existing methods.

COMPLIANCE WITH ETHICAL STANDARDS

The experimental procedures involving human subjects described in this paper were approved by the Institutional Review Board.

ACKNOWLEDGMENT

This work is supported in part by the National Key Technology Research and Development Program of China (No: 2017YFE0104000, 2016YFC1300302), and by the National Natural Science Foundation of China (No: U1809204, 61525106, 81873908, 61701436).

REFERENCES

[1] Wang L, Zhang H, Wong K C L, et al. Physiological-model-constrained noninvasive reconstruction of volumetric myocardial transmembrane potentials. IEEE Transactions on Biomedical Engineering, 2009, 57(2): 296-315.

[2] Xu J, Dehaghani A R, Gao F, et al. Noninvasive transmural electrophysiological imaging based on minimization of total-variation functional. IEEE transactions on medical imaging, 2014, 33(9): 1860-1874.

[3] Xie S, Wang L, Zhang H, et al. Non-invasive reconstruction of dynamic myocardial transmembrane potential with graph-based total variation constraints. Healthcare technology letters, 2019, 6(6): 181-186.

[4] Dhamala J, Bajracharya P, Arevalo H J, et al. Embedding high-dimensional Bayesian optimization via generative modeling: Parameter personalization of cardiac electrophysiological models. Medical image analysis, 2020, 62: 101670.

[5] Mu L, Liu H. Cardiac Transmembrane Potential Imaging with GCN Based Iterative Soft Threshold Network. MICCAI2021(Accepted)

[6] Fischer G, Tilg B, Wach P, et al. Analytical validation of the BEM—application of the BEM to the electrocardiographic forward and inverse problem. Computer Methods and Programs in Biomedicine, 1998, 55(2): 99-106.

[7] Kamilov U S, Mansour H, Wohlberg B. A plug-and-play priors approach for solving nonlinear imaging inverse problems. IEEE Signal Processing Letters, 2017, 24(12): 1872-1876.

[8] He K, Zhang X, Ren S, et al. Deep residual learning for image recognition[C]//Proceedings of the IEEE conference on computer vision and pattern recognition. 2016: 770-778

[9] Wang X, Girshick R, Gupta A, et al. Non-local neural networks//Proceedings of the IEEE conference on computer vision and pattern recognition. 2018: 7794-7803.

[10] Zhang J, Ghanem B. ISTA-Net: Interpretable optimization-inspired deep network for image compressive sensing//Proceedings of the IEEE conference on computer vision and pattern recognition. 2018: 1828-1837.